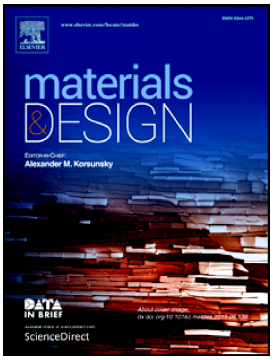

Buckling behavior of nanotubes from diamondene

Kun Cai, Lei Wang, Yi Min Xie

PII: S0264-1275(18)30237-5
DOI: doi:10.1016/j.matdes.2018.03.052
Reference: JMADE 3794

To appear in: *Materials & Design*

Received date: 28 January 2018
Revised date: 22 March 2018
Accepted date: 22 March 2018

Please cite this article as: Kun Cai, Lei Wang, Yi Min Xie , Buckling behavior of nanotubes from diamondene. The address for the corresponding author was captured as affiliation for all authors. Please check if appropriate. Jmade(2017), doi:10.1016/j.matdes.2018.03.052

Buckling behavior of nanotubes from diamondene

Kun Cai [1*], Lei Wang [2*], Yi Min Xie [1]

[1]*Centre for Innovative Structures and Materials, School of Engineering, RMIT University, Melbourne 3001, Australia*

[2]*Department of Engineering Mechanics, College of Mechanics and Materials, Hohai University, Nanjing 211100, China*

*Corresponding authors' email address: Kuncai99@163.com (K. C.); WangL@hhu.edu.cn (L. W.)

Abstract:

Under high pressure, two layers of graphene may have phase transition. After transition, a new two-dimensional material called as diamondene can be obtained, which recently has been verified by Raman spectra. As sp^2 & sp^3 composites, diamondene possesses both excellent mechanical properties and semi-conductivity. Similar to the carbon nanotube (CNT) from tailored graphene, a nanotube can also be made from a diamondene ribbon. In this study, the mechanical stability of diamondene nanotubes (DNTs) is investigated by theoretical analysis after molecular dynamics calculations. Results demonstrate that the minimal radius of a DNT without broken bonds is far greater than that of a single-walled CNT. Comparing to the double-walled CNTs with the same length and average diameter, DNTs behave more stable under uniaxial compression. Before collapse due to breakage of sp^3-sp^3 bond, a DNT has only one buckling mode. Under axial torsion, the wall of a DNT buckles at small torsion deformation. Between two edges of the nanotube, the shell becomes a warped ribbon at large torsion angle. During torsion, the number of broken bonds in the outer layer of DNT is far greater than that of the inner layer, and both numbers grow with the torsion angle. Few inter-layer bonds break due to the synchronous rotation of two layers in torsion.

Keywords: carbon nanotube, diamondene, mechanical stability, molecular dynamics

1. Introduction

In periodic table, carbon is the sixth element with electron configuration of $2s^2p^2$, and has many allotropes. For example, fullerene, a carbon nanoball found in 1985 [1, 2], can be considered as 0-dimensional structure. In one-dimensional style, carbon nanotubes (CNTs) have been found in electron microscope for over a quarter of century [3]. Now, CNTs are popular in nanodevices [4-12]. In the earlier of this century, Novoselov, Geim et al. [13, 14] had obtained few-layered graphene. Further research results indicate that the new two-dimensional material behaves excellent physical properties [15-19]. People still believe that graphene has wide potential application in nanodevices [20, 21]. For a three-dimensional carbon structure, diamond is well-known, and has been used in engineering with regard to its extremely high hardness and light transmission. All the unique properties of the carbon materials rely on their own electron structures.

Besides the allotropes of carbon found in nature, people also predict new carbon structures according to the possible electron structures, e.g., line of sp, plane of sp^2 and tetrahedron of sp^3. For instance, Xu et al. [22] built a 3-dimensional network carbon structure by combing graphene and CNTs, and investigated the thermal and mechanical performance of the nano network. Varshney et al. [23] developed a computational framework to model a variety of junction structures between CNTs with arbitrary spatial and intrinsic specification and this method can easily be extended to build multi-junction nanotube clusters, multi-wall nanotube junctions, as well as 3D random network structures. Yang et al. [24] designed a hybrid carbon matrix using 3D interconnected porous carbon nanosheet and CNTs for high performance lithium-sulfur batteries with rapid electron/ionic transport. Recently, Jiang et al. [25] suggested a new carbon allotrope, named twin graphene. The new 2-dimensional material is a semiconductor with bandgap dependent on strain. Martins et al. [26]

reported a new 2-dimensional material by putting two layers of graphene at high pressure. They called the new carbon material as diamondene because of its sp^2+sp^3 composited structure. Gao et al. [27] also demonstrated a diamond-like ultra-hard structure transformed from multilayer graphene. Rather than graphene behaving as an excellent conductor or diamond as an insulator, according to their results, diamondene behaves as a ferromagnetic semiconductor with spin polarized bands. It implies that the new 2-dimensional material possesses both the excellent mechanical properties and semi-conductivity. In diamondene, a carbon atom has either 3 sp^2 or 4 sp^3 electrons. The two wavy sheets of diamondene are covalently bonded by sp^3 atoms. It is easily to predict that the in-plane elastic modulus of diamondene is less than that of graphene. However, due to stronger bonding interaction between the two layers in diamondene than the nonbonding interaction between two layers of graphene, the out-of-plane bending stiffness of diamondene must be far greater than that of a monolayer graphene.

Excellent toughness of CNTs can guarantee the CNT structures working safely. Besides, it also may provide fascinating applications. For example, Foroughi et al. [28] reported an electrolyte-filled twist-spun carbon nanotube yarn which serves as a torsional artificial muscle providing reversible 15,000° rotation and 590 revolutions per minute. Subsequently, Lima et al. [29] designed guest-filled, twist-spun carbon nanotube yarns as electrolyte-free muscles that provide fast, high-force, large-stroke torsional and tensile actuation. In 2017, based on CNTs, Kim et al. [30] made a continuous step on electrical energy harvesting devices which convert tensile or torsional mechanical energy into electrical energy without requiring an external bias voltage. These energy harvesters can be widely used in ocean wave energy harvesting, thermally driven artificial muscle, self-powered sensors, etc.

In the present study, we investigate the stability of a nanotube made from diamondene. From geometrical point of view, a carbon nanotube can be considered as a curved rectangular graphene [31, 32]. Hence, we predict that the new one-dimensional material, i.e., diamondene nanotube (DNT), can be fabricated for potential application in NEMS. But before application, we need to make a deep understanding of DNTs' properties. In this study, we propose an expansion-shrinkage method to build DNTs from two coincident CNTs. By molecular dynamics (MD) simulations, we predict the maximal curvature of an armchair or zigzag diamondene nanotube (A-/Z-DNT). Further, we focus on the mechanical stability of such new one-dimensional material under axial compression or torsion. To avoid the influence of thermal vibration of carbon atoms and to capture the essential mechanical characteristics of nanotubes from diamondene, a low temperature of 1K is chosen for all simulations in the present work.

2. Models and method

2.1 Models

In Figure 1, three views of a diamondene ribbon and the DNTs are illustrated. To figure out the relative positions of the atoms on both layers, the atoms in the bottom layer or outer layer of DNT (Figure 1d or e) are set to black. The atoms in the other layer are set to yellow. For convenience of comparison between DNTs and the normal CNTs as shown in Figure 1f, g, the atoms in the outer and the inner CNT are set to blue and red, respectively. Figure 1 only gives four short nanotubes. In the following stability tests, we need nanotubes whose axial lengths are of ~15nm. The parameters of the four nanotubes involved in analysis are listed in Table 1.

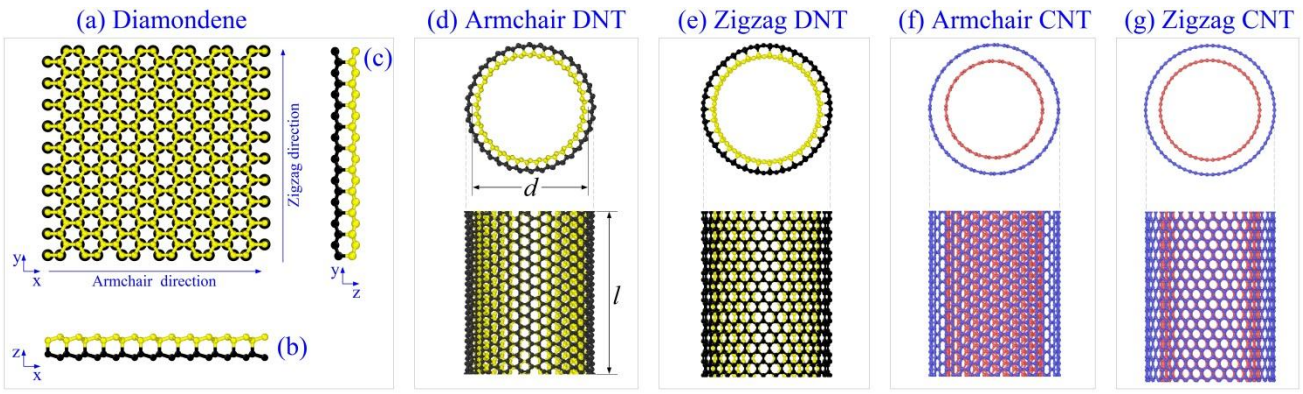

Figure 1Geometry of diamondene and nanotubes. (a) a diamondene ribbon in x-y plane; (b) view of ribbon in x-z plane; (c) view of ribbon in y-z plane; (d) armchair (A-) diamondene nanotube with average diameter of *d* and axial length of *l*, its chirality is of ((18,18)); (e) zigzag (Z-) diamondene nanotube with chirality of ((31, 0)); (f) double-walled armchair carbon nanotube with chirality of (15, 15)/(20, 20); (g) double-walled zigzag carbon nanotube with chirality of (27, 0)/(35, 0).

Table 1Parameters of four nanotubes with similar initial diameters (*d*) in Figure 1. In loading tests, *l** is the effective length of nanotube, which is slightly lower than the total length of tube, i.e., *l*. Slenderness ratio equals *l**/*d*. Dimension unit: nm.

Pattern	Chiral index	*r*	*d*=2*r*	*l*	*l**	Slenderness
Armchair DNT	((18, 18))	1.245	2.49	15.95	14.95	6.00
Zigzag DNT	((31, 0))	1.24	2.48	15.52	14.65	5.91
Armchair CNT	(15, 15)/(20, 20)	1.24	2.48	15.95	14.95	6.03
Zigzag CNT	(27, 0)/(35, 0)	1.24	2.48	15.52	14.65	5.91

2.2Modeling of a DNT from CNTs

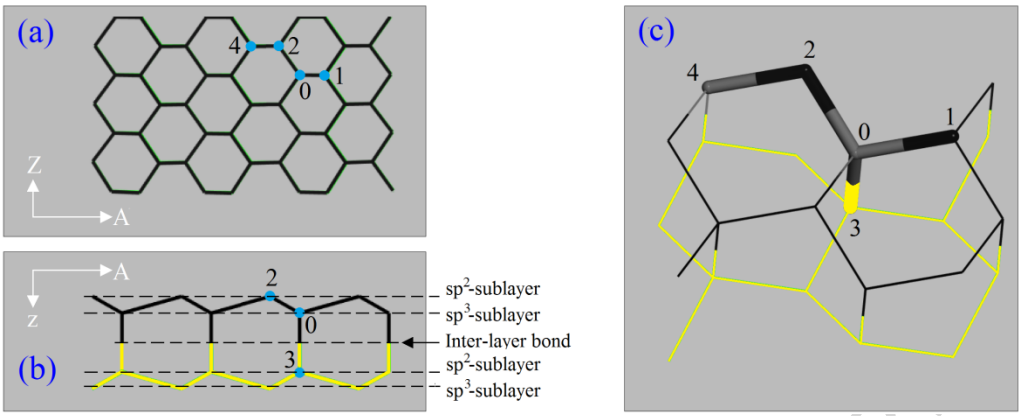

Figure 2Representative atoms in a DNT. A-direction is of the circumferential direction of an armchair DNT (A-DNT), or of the generatrix of a zigzag DNT (Z-DNT). (a) Local side-view of DNT, (b) Local axial-view of DNT, (c) oblique-view of a segment of DNT.

Before building a DNT, we need to illustrate the positions of atoms in both layers in either diamondene or DNT. Diamondene is a sp^2+sp^3 composites, in which the sp^2 atoms (e.g., atoms 1 and 2 in Figure 2) and sp^3 atoms (e.g., atoms 0 and 3) have the same number and they distribute uniformly in each layer of diamondene. The 2-layered two-dimensional structure has a symmetric plane as shown in Figure 2b. From the side-view of DNT, i.e., Figure 2a, it has similar honeycomb structure and the two vertical directions of armchair and zigzag directions are marked as "Armchair (A) direction" and "Zigzag (Z) direction" in Figure 1a-c, respectively. Lower case "z", i.e., the thickness direction of diamondene in Figure 1b-c, represents the reversely radial direction. The atoms in the bottom layer, e.g., 0, 1, 2 and 4, are set to black, and the atoms in the upper layer are set to yellow.

Two approaches are available to form the geometry model of a DNT from diamondene. One is the geometry mapping method [33], in which the Cartesian coordinates of the atoms in a rectangular

diamondene are mapped into cylindrical coordinates. In the present work, we propose another method to obtain DNTs. In the so-called expansion-shrinkage method, four steps are required to obtain a DNT from CNTs.

First, prepare two identical CNTs, i.e., both having chiral index as (18, 18) for A-DNT or (31, 0) for Z-DNT. Initially, the two tubes are completely coincident;

Second, shrink the inner (yellow) layer: the average radius of sp^3-sublayer reduces 8%, and the radius of the sp^2-sublayer reduces 12%;

Third, expand the outer (black) layer: the average radius of the sp^3-sublayer increases 8%, and the radius of the sp^2-sublayer increases 12%. In the initial configuration of the DNT, the inter-layer bond lengths are identical to 0.16nm;

Final, minimize the potential energy of the system to obtain the initial configuration of a DNT for mechanical experiments.

2.3 Schematic of loading tests

Figure 3 illustrates two loading cases for testing the stability of the DNTs with parameters listed in Table 1. Under uniaxial compression, the bottom edges of the layers of tube are fixed of the degrees of freedom, and the upper edges of the tube moves downward with velocity v (Figure 3a), i.e., moves 0.001nm and followed with 3,000 steps of relaxation. The motion of the upper edges of the tube stops when the tube has serious buckling. Under axial torsion, the bottom edges of the tube are fixed with their degrees of freedom, and the upper edges has an identical rotational speed, i.e., in each step the increment of θ (Figure 3b), i.e., ω, is 0.5° and followed with 3,000 steps of relaxation. The

rotation stops when the tube has serious of deformation. Details are given in next section.

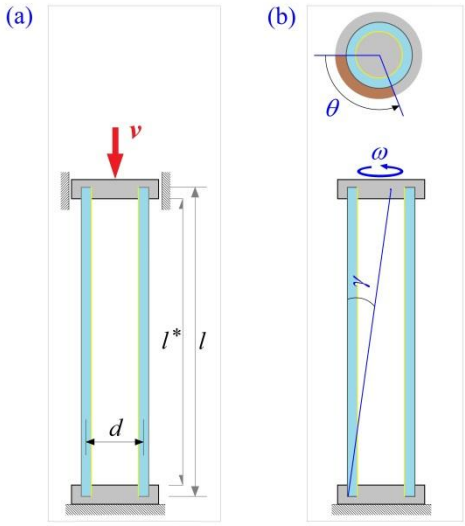

Figure 3Schematics of two types of loading on a nanotube. (a) Uniaxial compression with the bottom of tube(s) being fixed. The value of **axial strain** of tube equals the relative difference between the current and initial lengths divided by the initial length. (b) Axial torsion. In torsion, the bottom edges of tubes are fixed, and torque speed ω is applied on the top edges. θ is the **torsion angle** of the edges with the shear angle of γ.

2.3 Method of MD simulation

The update of motions of the atoms in a nanotube under loading are fulfilled by the open source code LAMMPS [34]. Seven major steps are contained in each simulation, i.e.,

Step 1: Build a nanotube, either DNT or double-walled CNTs;

Step 2: Reshape the nanotube in a cube with side length of 40nm by energy minimization;

Step 3: Keep 200,000 steps of relaxation of the system at canonical (NVT) ensemble with T=1K;

Step 4: Fix the atoms at the bottom of the tube(s);

Step 5: Start loading at NPT ensemble, i.e., the top edges moves downward 0.001nm with 3,000 steps of relaxation, or rotates 0.5° with 3,000 steps of relaxation;

Step 6: Collect data during loading for post-processing. If the tube has serious deformation, go to Step 7, otherwise go to Step 5;

Step 7: Stop and start post-processing.

In simulation, the increment of time is 0.001ps, and the interaction among the carbon atoms is evaluated by AIREBO potential [35], which contains three items, i.e.,

$$\begin{cases} P = P_{\mathrm{REBO}} + P_{\mathrm{Torsion}} + P_{\mathrm{L\text{-}J}} \\ P_{\mathrm{REBO}} = \sum_i \sum_{j(j>i)} \left[V_{ij}^R(r_{ij}) - b_{ij} V_{ij}^A(r_{ij}) \right] \\ P_{\mathrm{Torsion}} = \frac{1}{2} \sum_i \sum_{j(j\neq i)} \sum_{k(k\neq i,j)} \sum_{l(l\neq i,j,k)} w_{ij}(r_{ij}) \cdot w_{jk}(r_{ij}) \cdot w_{kl}(r_{ij}) \cdot V_{\mathrm{Torsion}}(\omega_{ijkl}) \\ P_{\mathrm{L\text{-}J}} = \sum_i \sum_{j(j>i)} 4\varepsilon \left[\left(\frac{\sigma}{r_{ij}} \right)^{12} - \left(\frac{\sigma}{r_{ij}} \right)^{6} \right] \end{cases} \tag{1}$$

where P_{REBO} represents the short-range REBO potential with impulsive part V_{ij}^R and attractive part V_{ij}^A with respective to atom types of atoms i and j. r_{ij} is the distance between atoms i and j, and b_{ij} illustrates the bond-order effect. P_{Torsion} depends on the dihedral angle ω of the atoms i, j, k, and l, with bond weights (w_{ij}) in [0, 1], and V_{Torsion} is the atom-based dihedral-angle potential. $P_{\mathrm{L\text{-}J}}$ is the Lennard-Jones potential [36] to describe the non-bonded intermolecular interactions with parameters of $\sigma_{C\text{-}C}$=0.34nm, $\varepsilon_{C\text{-}C}$=2.84meV, and the cutoff 1.02 nm.

Eq.(1) says that the potential energy of a carbon nanostructure depends on the relative positions of atoms. When the configuration of the system changes in simulation, the variation of potential energy (VPE) exists, and can be defined as:

$$\mathrm{VPE}=P(t)\text{-}P(t_0), \tag{2}$$

where $P(t)$ and $P(t_0)$ are the potential energy of the system at time t and t_0, respectively. When t_0 is the initial moment, the value of VPE represents the total variation of potential energy. In this study, we adopt this value to demonstrate the change of configuration of a nanotube.

To show the stiffness, we also calculate the axial stress. In LAMMPS, the local stress tensor of each atom is calculated based on a Virial style definition [37]. The volume involved in calculation is defined as the volume of the simulation box, i.e., 40nm×40nm×40nm. The averaged value of the axial components of all the unfixed atoms in tube is of the axial stress of tube.

3. Results and discussion

3.1 Critical curvature radii of DNTs

Comparing to graphene, diamondene has a higher thickness with two bonded layers. Hence, it must have a higher out-of-plane bending stiffness than graphene. When we consider a CNT made from curved graphene, the chiral index of a CNT can be as small as (3, 4). However, for a DNT, its chiral index cannot be so small. The reason is that the sp^3-sp^3 bonds in the outer layer of DNT are under serious stretching while the bonds in the inner layer under compression. When the curvature radius of a DNT is too small, some of the sp^3-sp^3 bonds may have to be broken to reduce the potential energy of the system, which means the broken DNT is in a more stable state.

Using MD simulation, we test the chiral index of DNTs without broken sp^3-sp^3 bond. For example, except the edges, the DNT ((15, 15)) has no sp^3-sp^3 bond in the outer layer after full relaxation (Figure 4). In the case of DNT ((18, 18)), there is no broken sp^3-sp^3 bond during relaxation. After relaxation, the radius of ((18, 18)) is ~1.295nm, which is ~4.4% higher than the initial radius listed in

Table 1. For a zigzag DNT with small radius, e.g., ((26, 0)), lots of sp^3-sp^3 bonds on it are broken at both edges (see inset in Figure 4). Whilst, the DNT ((31, 0)) has no broken sp^3-sp^3 bond during relaxation, and its radius after relaxation is of ~1.289 nm, which is ~4% higher than the initial radius listed in Table 1. The drop of VPE with respect to ((18, 18)) or ((31, 0)) are caused by the reshape of the nanostructure during relaxation with free edges.

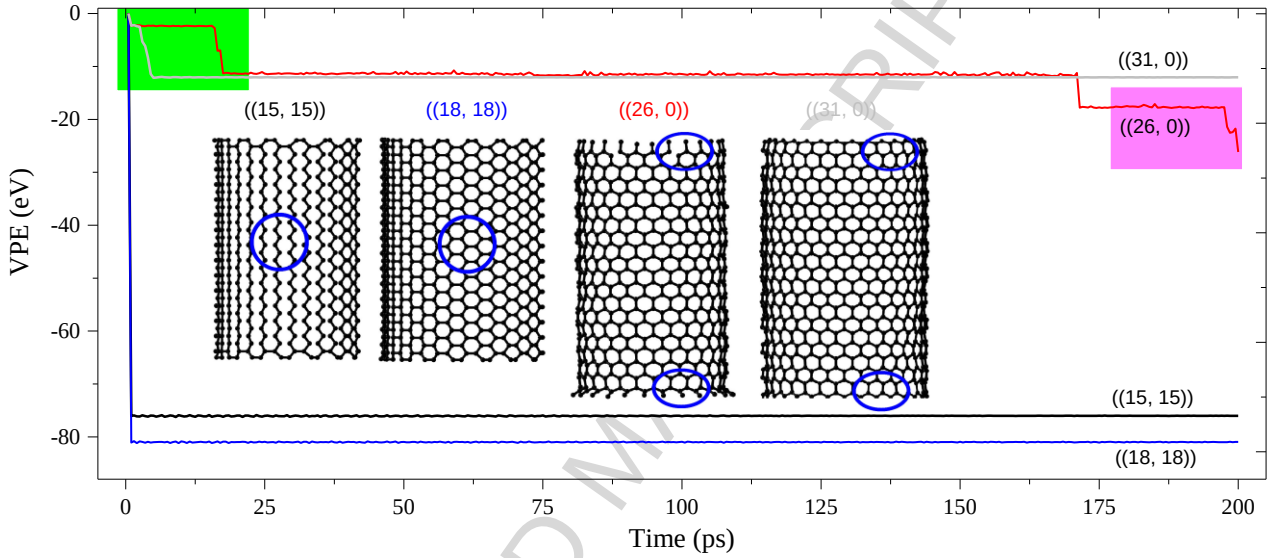

Figure 4Variation of potential energy (VPE) of four DNTs during relaxation. The inset shows the configuration of the outer layers of the tubes at 200ps. The initial axial length of the armchair tubes is of ~3.77nm. The initially axial length of the zigzag tubes is of ~4.35nm. The potential energy of the initial tubes are of -11134.6eV of DNT ((15, 15)), -13492.0eV of ((18, 18)), -13177.1eV of ((26, 0)), and -15895.1eV of ((31, 0)), respectively.

Meanwhile, the change of the tube's axial length is mainly due to the shrink of its edges. For example, without considering both edges, the initial and final lengths of the DNT ((15, 15)) are ~3.448nm and ~3.449nm, respectively. For the DNT ((18, 18)), its initial and final axial length are ~3.440nm and ~3.447nm, respectively. For the zigzag DNTs, ((26, 0)) has the same initial and final lengths of

3.868nm. The initial and final lengths of ((31, 0)) are ~3.872nm and ~3.876nm, respectively. Hence, only the tube's edges are reshaped slightly during relaxation. The difference between two armchair DNTs or zigzag DNTs is cause by their different curvatures.

3.2 Buckling behavior of DNTs under uniaxial compression

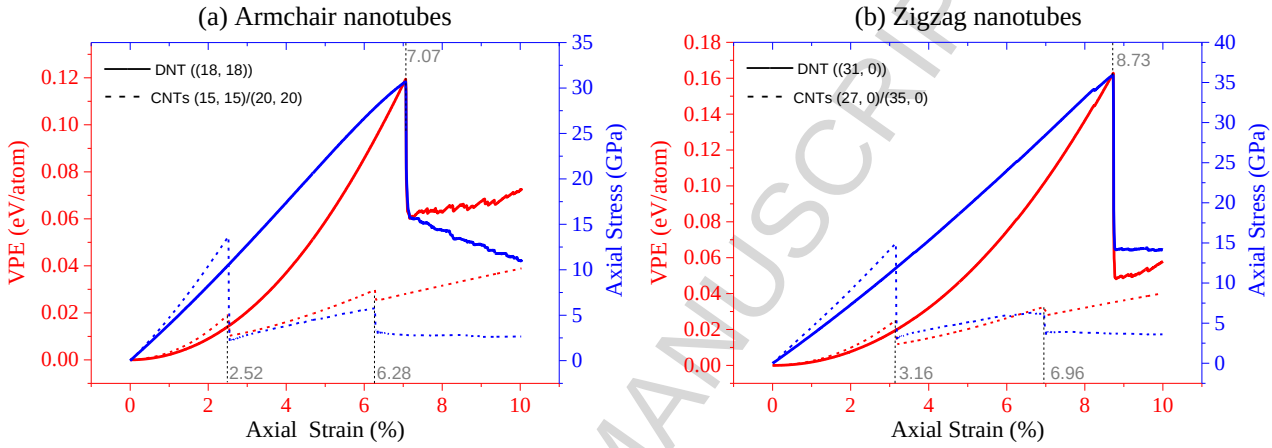

Figure 5Deformation potential energy (red curves) and axial stresses (blue curves) of four different nanotubes. (a) Armchair type: DNT ((18, 18)) vs. CNTs (15, 15)/(20, 20); (b) Zigzag type: DNT ((31, 0)) vs. CNTs (27, 0)/(35, 0). Solid curves are for DNTs, and broken lines for CNTs.

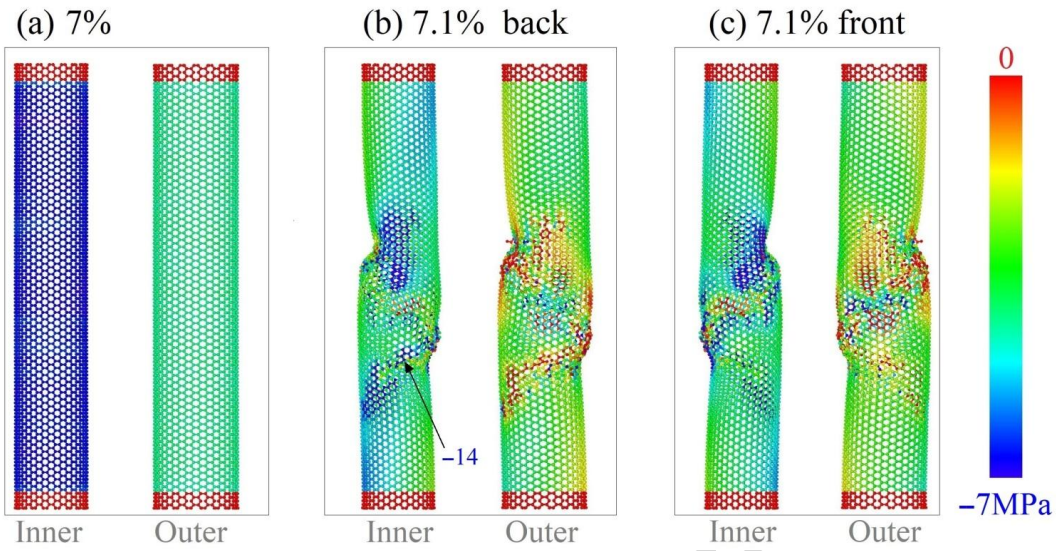

Figure 6 Contour plot of local axial stress component of atoms in ((18,18)) DNT with different axial stains prior to and after buckling occurs.

By putting the four types of nanotubes under compression, we draw the curves of the VPE and stress vs. engineering strain as shown in Figure 5. For the armchair models (Figure 5a), the peak value of stress of the A-DNT, i.e., buckling stress, is over 30GPa at 7.07%, which is far greater than ~14GPa of the A-CNTs at strain of 2.52%. Therefore, we conclude that the stability of the DNT is far greater than that of the double-walled CNTs with similar average diameter. The reason is that the bonding interaction between two layers in the DNT is much stronger than the non-bonding interaction between the two tubes in CNTs. Hence, the bending stiffness of the 2-layered shell is higher than that of the two tubes in the CNTs when they have similar slenderness. However, before buckling, e.g., axial strain less than 2.52%, the axial stress increases linearly, which means that the elastic modulus of CNTs is ~555.5GPa. And the elastic modulus of the DNT is ~ 424.3GPa, which is ~31% less than that of the CNTs, which means the CNTs have higher stiffness than the DNT before buckling of the CNTs.

Figure 6 illustrates the distribution of atoms stress in each layer of the ((18,18)) DNT having different axial deformation. Except both edges of each layer in the ((18,18)) DNT, the stress fields in both layers are uniform when the axial strain is 7% (Figure 6a). But, when the axial strain has a small increasing, e.g., 7.1%, both layers have drastic deformations at the middle parts. The stress fields fluctuate at the severely deformed areas. And the peak stress appears at the concave area in the inner layer (thinner tube in Figure 6b/c). The reason is that the atoms are under complicated compression from three orthogonal directions. The maximum compressive stress, i.e., -14MPa, appears at the middle part of the inner layer with axial strain of 7.1%.

According to the snapshots shown in Figure 7a, we know that the A-DNT has only axial deformation when the strain is less than 7.07%. However, both layers of the DNT are seriously damaged when the axial strain grows slightly to be 7.1%. Table 2 lists the changes of bond numbers in the DNT. It says that 478 bonds in the outer layer in the A-DNT break at strain of 7.1% (Movie 1). Meanwhile, the inner layer has 22 broken bonds, and 80 bonds connecting both layers break. Commonly, breakage of a covalent bond leads to increasing of the potential energy of the system. But the VPE curve shown in Figure 5a indicates that the value of VPE drops suddenly. It means that such number of broken bonds does not result in increasing of the total potential energy. The reason is that both items of P_{Torsion} and $P_{\text{L-J}}$ in Eq.(1) decrease during the breakage of the bonds. For the whole structure, the deformation potential energy releases after breakage. When the axial strain is higher than 7.1%, the stress of the DNT is dropping slowly. It means that the tube fails to support loading.

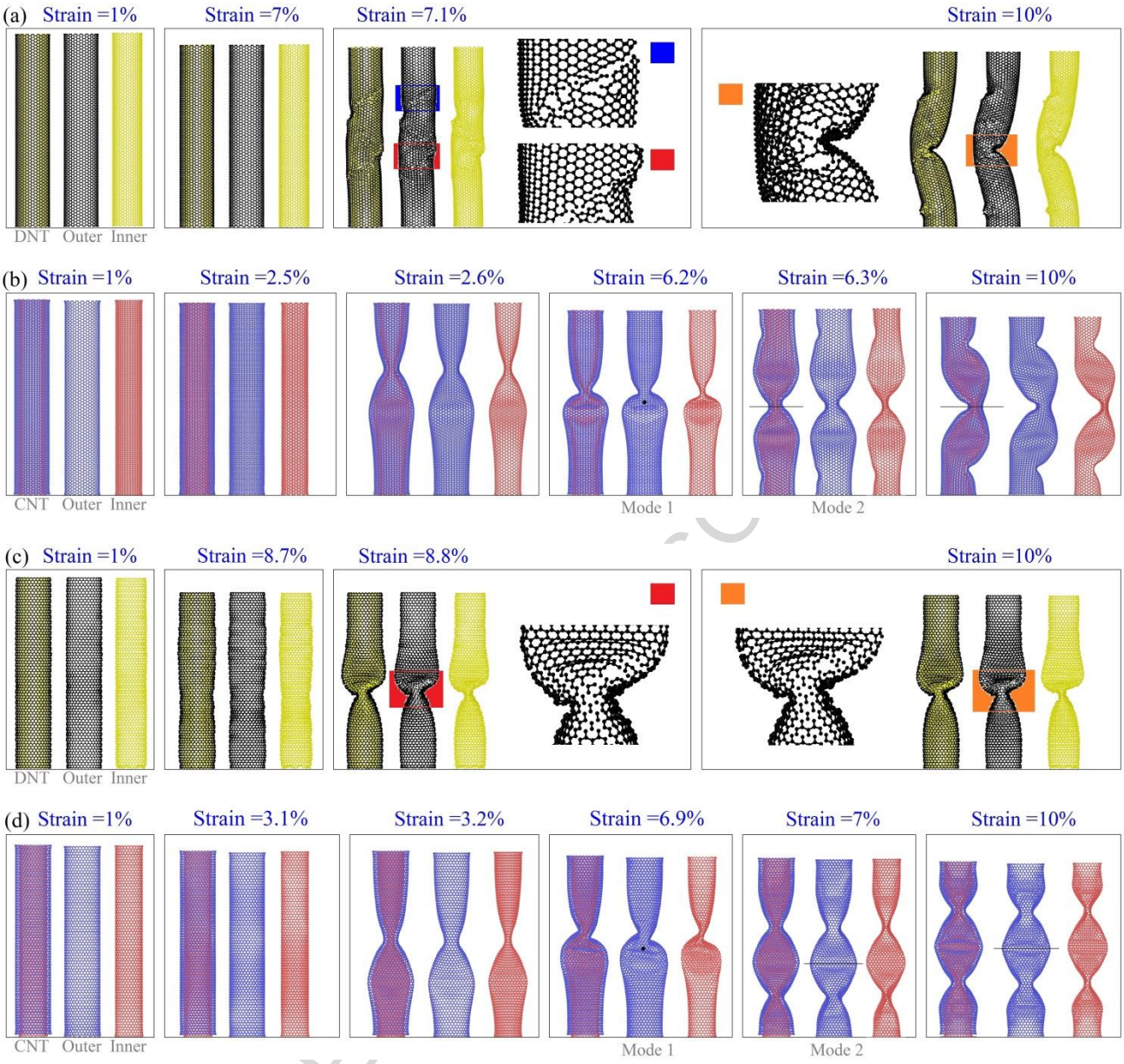

Figure 7 Representative snapshots of nanotubes during uniaxial compression. (a) Armchair DNT, (b) armchair CNT; (c) zigzag-DNT, (d) zigzag-CNT. Each group contains three tubes, and their names are labeled below at stain of 1%. For example, in (a), the first one is a DNT, the second tube in black is the outer layer of the DNT, and the third tube in yellow is the inner one. Each CNT has two modes during buckling.

Figure 7b illustrates that the A-CNTs have no damage even it has serious deformation. The first drop

point of stress at strain of 2.52% in Figure 5a is caused by the first-ordered buckling of the tubes. The related mode, i.e., the first-ordered mode which is symmetric about a point, keeps slight change before the axial strain approaching 6.28%. The second-ordered mode, which has a symmetric plane, appears when the strain is over 6.28% (Movie 2). Even when the axial strain approaches 10%, the mode does not change further. According to the decreasing of stress of the CNTs with strain higher than 6.28%, the nanostructure fails to support load. But different from the A-DNT, the CNTs can return to its original shape when releasing the external load.

Figure 7c gives the representative snapshots of the Z-DNT under compression. The tube buckles at the axial strain of 8.73%, which is ~23% higher than that of the A-DNT in Figure 5a. The first-order mode is very clear even the outer layer has serious damage (Movie 3). The decreasing of stress shown in Figure 5b demonstrates that the tube does not support further loading any more. In fact, Table 2 indicates that the breakage of inter-layer bonds starts before the strain approaching 8%. The reason is that the sp^3-sp^3 bonds in the outer layer are layout along the circumferential direction, and they have slight deformation during loading.

Figure 7d gives some snapshots of the Z-CNTs, which has the first-ordered buckling at axial strain of 3.16%, and the second-ordered buckling at strain of 6.96%. The tubes cannot bear loading when the strain is over 7%. Having no broken C-C bond during compression indicates the CNTs have excellent elasticity.

Table 2 Number of C-C bonds in A-DNT ((18, 18)), and Z-DNT ((31, 0)) at different axially compressive strains. In calculating the bond numbers, both atoms with distance less than 0.17nm can be considered as covalently bonded.

Model		Strain=0	2%	4%	6%	7%	7.1%	8%	9%	10%
A-DNT	Inner layer	13752	13752	13752	13752	13752	**13730**	13690	13674	13670
	Outer layer	13712	13682	13680	13680	13680	**13202**	13104	12914	12850
	Inter-layer	4608	4608	4608	4608	4608	**4528**	4496	4468	4458
		Strain=0	2%	4%	6%	7%	8%	8.5%	9%	10%
Z-DNT	Inner layer	13330	13330	13330	13330	13330	13330	13330	**13320**	13314
	Outer layer	13330	13330	13330	13330	13330	13330	13330	**12704**	12552
	Inter-layer	4402	4402	4402	4402	4402	**4394**	4342	**3850**	3772

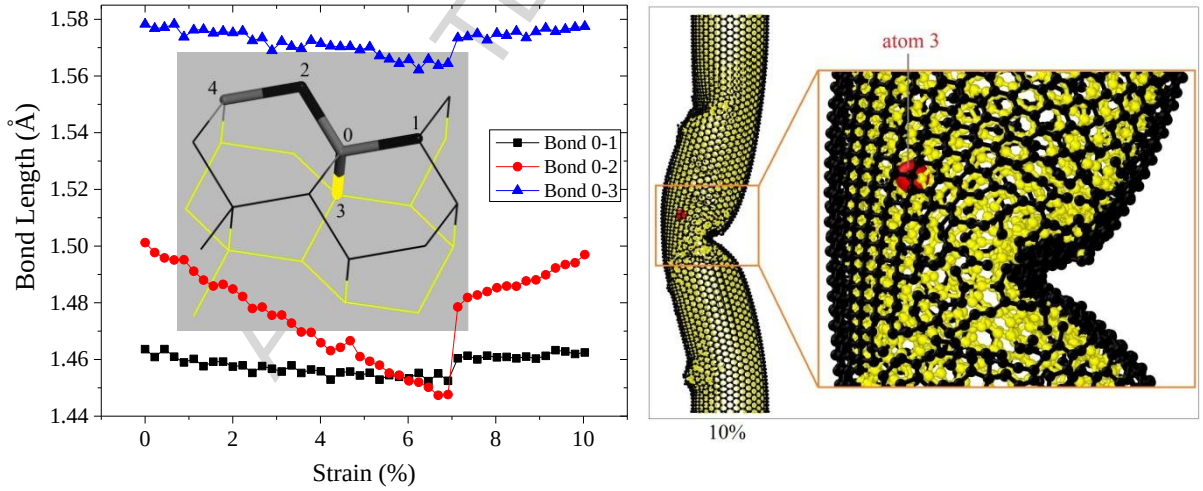

Figure 8 Length variations of representative bonds (Figure 2c) with the increase of axial compressive strain in ((18, 18)) DNT. Right is the configuration of ((18,18)) DNT with strain of 10%.

During compression, the bond lengths vary at different speeds. Figure 8 gives the length histories of the three representative bonds in the ((18,18)) DNT. Bond 0-3 is the inter-layer bond which describes the state of atoms 0 and 3. For example, when the length of bond 0-3 is higher than 1.7nm, we consider that the covalent interaction between atoms 0 and 3 can be neglected, and the bond can be considered to be broken. From the history of length of bond 0-3, we find that the atoms 0 and 3 are well covalently bonded during compression. From the configuration of the DNT at 10%, we find that the local bonds nearby atom 3 (red ball) are not broken. The length of bond 0-1 changes slightly during compression. Only bond 0-2 reduces obviously during compression. Meanwhile, we also find that before 7% of axial strain, the bond lengths change continuously. But at 7.1%, the lengths of the three bonds jump up to their initial values rapidly. The reason is that the buckling deformation nearby atom 3 leads to energy releasing of the rest area.

3.3 Buckling behavior of DNTs under torsion

When a thin-wall shell is under axial torsion, it also may buckle due to compression of stress along the helix angle of 45° of the shell. The buckling state depends on the relative torsion angle of both edges. Figure 9 gives four VPE curves of four nanotubes under axial torsion. For the armchair nanotubes, DNT is in buckling state at the torsion angle of 57° (the related snapshot can be found in Figure 10a). When torsion angle increases, the VPE curves have more drop points, which imply that the configuration of the tube changes frequently (Movie 4). For example, the snapshot with respect to 229° is obviously different from the previous configuration with respect to 57°. The middle part of the tube has serious deformation, and looks like a warped ribbon. One can find that a small part of the tube has been damaged. When the torsion angle is higher than 286°, the warped ribbon begins

breaking. Table 3 tells the truth is that large number of C-C bonds in the outer layer has broken at such high distortion. It can be found that the number of inter-layer bonds changes slightly. The reason is that the shear deformation of both layers happens simultaneously, which leads to the inter-layer bonds having small deformation.

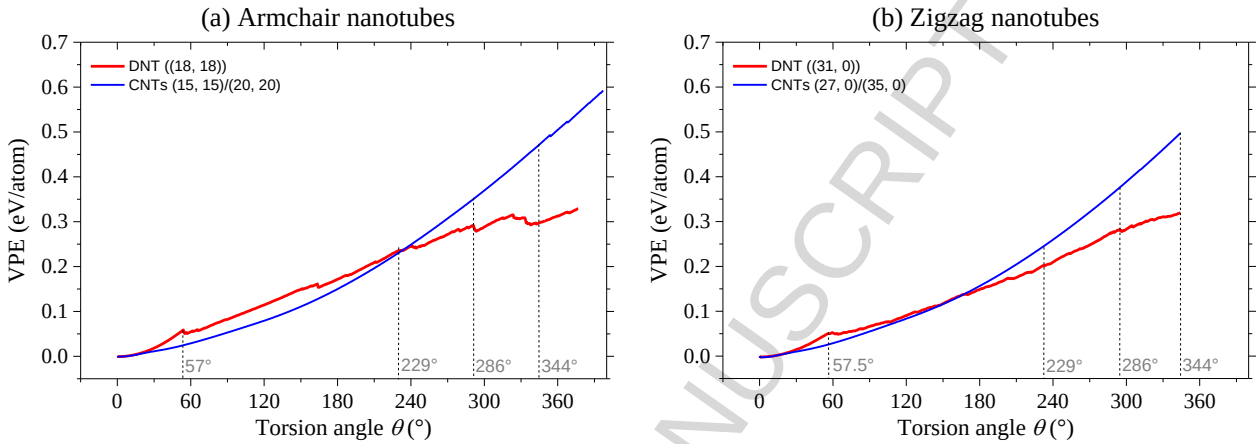

Figure 9 VPE of nanotubes in different axial torsion angle θ. (a) Armchair type: DNT ((18, 18)) vs. CNTs (15, 15)/(20, 20); (b) Zigzag type: DNT ((31, 0)) vs. CNTs (27, 0)/(35, 0). Curves in red and blue are for DNTs and CNTs, respectively.

Comparing to the A-DNT, the A-CNTs having serious deformation (Figure 10b) has lower number of broken C-C bonds in the outer layer. For example, there are only 6 broken bonds in the A-CNTs at the torsion angle of 229°. When θ is higher than 229°, the number of broken bonds grows rapidly, e.g., 324 at 286°, 1540 at 344° in Table 3, respectively.

In Figure 10c, some snapshots of the Z-DNT with different values of θ are given. The tube becomes buckle before θ approaching 57°. The configuration of the tube changes with the increasing of θ. When θ is no higher than 286°, the outer layer has some small local damages. At θ=344°, the tube damages seriously, and is not rotational symmetric any more. According to the data listed in Table 3,

both layers have lots of broken bonds. For example, the outer layer has 1970 broken bonds when θ=144°. Simultaneously, the inner layer has 302 broken bonds and inter-layer connection has 586 broken bonds.

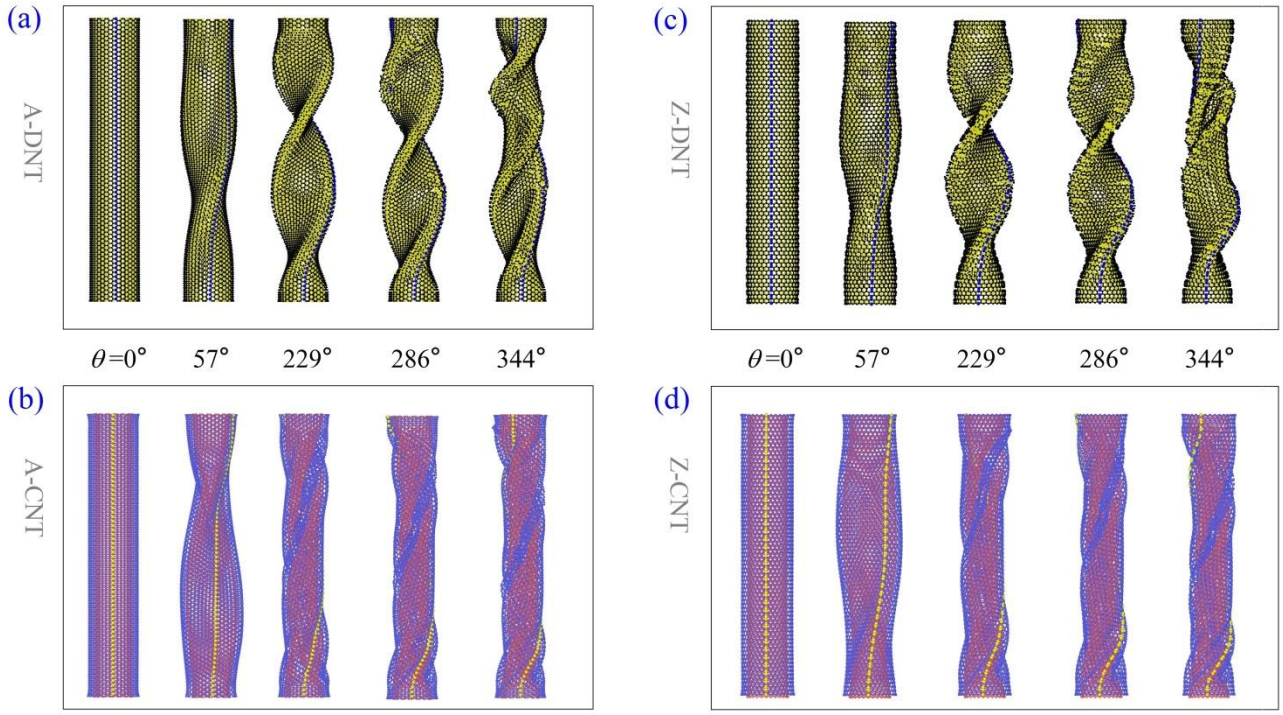

Figure 10 Representative snapshots of nanotubes at different torsional angles. (a) armchair DNT, (b) armchair CNT; (c) zigzag-DNT, (d) zigzag-CNT.

Table 3 Number of C-C bonds in DNTs at different axial torsion angles. In calculating the bond numbers, both atoms with distance less than 0.17nm can be considered as covalently bonded.

Model		θ=0°	29°	57°	86°	115°	144°	159°	173°
A-DNT	Inner layer	13752	13752	13890	13978	14028	**14074**	14088	14050
	Outer layer	13704	13688	12476	12104	11722	**11302**	10988	10904
	Inter-layer	4608	4608	4610	4606	4570	**4568**	4548	4550
		θ=0°	29°	57°	86°	115°	144°	159°	173°
Z-DNT	Inner layer	13330	13330	13322	13240	13140	**13028**	12984	12918
	Outer layer	13330	13300	12098	11826	11606	**11360**	11144	11030
	Inter-layer	4402	4402	4318	4096	3940	**3816**	3752	3714

For the snapshots of the Z-CNTs shown in Figure 10d, the Z-CNTs has different buckling mode from the A-CNTs in Figure 8b when θ=57°. But the difference decreases with the increasing of θ. For example, the statistics results show that the CNTs have 2 broken bonds at θ=286°, and have 330 broken bonds at θ=344°.

4. Conclusions

Diamondene behaves as a ferromagnetic semiconductor, which means wide potential application of diamondene in nano-electro-mechanical systems. Using expansion-shrinkage method, we build geometry model of DNTs from two coincident CNTs. By molecular dynamics simulations, the maximal curvature of an armchair or zigzag DNT is evaluated. The compression and torsion tests are

fulfilled. Some concluding remarks on the stability of DNTs at 1K are made as following,

(1) The armchair DNT ((18, 18)) with radius of ~1.295nm can be considered as the minimum radius of the armchair DNTs in stable state. For a stable zigzag DNT, its radius should be no less than 1.289nm.

(2) In uniaxial compression tests, stability of a DNT is far greater than that of the double-walled CNTs with similar average diameter because of the bonding interaction between two layers in the DNT stronger than the non-bonding interaction between the two tubes in a CNT.

(3) In compression, DNT fails to support loading after the first-ordered buckling. Whilst, the double-walled CNTs has two buckling modes before failure. Before buckling, the outer layer of armchair DNT has damaged even if the axial strain is only 2%. But the zigzag DNT does not break even after buckling with axial strain of 8.5%.

(4) In axial torsion of the nanotubes, they start buckling at small shear deformation. After buckling, the tube has serious deformation between two fixed edges, and looks like a warped ribbon when the rotational angle is higher than 229° with respect to the axial length of ~15nm.

(5) During torsion of the DNTs, the number of broken C-C bonds in the outer layer is much higher than that in the inner layer, and the inter-layer bonds changes slightly due to both layers has synchronous rotation.

Acknowledgements

The authors declare no competing financial interests. Financial support from National Natural Science Foundation, China (Grant No.: 51505388, 11472098), and National Key Research and Development Plan, China (Grant No.: 2017YFC0405102) are acknowledged.

Supporting materials

Movies:

Movie 1-A-DNT with compressive strain in [0.07, 0.071].avi

Movie 2-A-CNT with compressive strain in [0.062, 0.063].avi

Movie 3-Z-DNT with compressive strain in [0.087, 0.088].avi

Movie 4-A-DNT with torsion angle in [0, 229] degree.avi

Data Availability

The raw/processed data required to reproduce these findings cannot be shared at this time as the data also forms part of an ongoing study.

References

1 Kroto HW, Heath JR, Obrien SC, Curl RF, Smalley RE. C60: Buckminsterfullerene. *Nature*, 1985, **318**(6042): 162–163.

2 The Nobel Prize in Chemistry 1996, https://www.nobelprize.org/nobel_prizes/chemistry/laureates/1996/, (Retrieved Dec. 21, 2017)

3 Iijima S. Helical microtubules of graphitic carbon. *Nature*, 1991, **354** (6348):56–58.

4 Cumings J, Zettl A. Low-friction nanoscale linear bearing realized from multiwall carbon nanotubes. *Science, 2000*, **289** (5479):602–604.

5 Treacy MMJ, Ebbesen TW, Gibson JM. Exceptionally high Young's modulus observed for individual carbon nanotubes. *Nature*, 1996, **381**(6584): 678–680.

6 Zheng QS, Jiang Q. Multiwalled carbon nanotubes as gigahertz oscillators. *Phys. Rev. Lett.*, 2002, **88**(4):045503.

7 Guo WL, Guo YF, Gao HJ, Zheng QS, Zhong WY. Energy dissipation in gigahertz oscillators from multiwalled carbon nanotubes. *Phys. Rev. Lett.*, 2003, **91**(12):125501.

8 Legoas SB, Coluci VR, Braga SF, Coura PZ, Dantas SO, Galvao DS. Molecular-dynamics simulations of carbon nanotubes as gigahertz oscillators. *Phys. Rev. Lett.*, 2003, **90**(5):055504.

9 Barreiro A, Rurali R, Hernandez E R, Moser J, Pichler T, Forro L, Bachtold A. Subnanometer motion of cargoes driven by thermal gradients along carbon nanotubes. *Science*, 2008, **320**(5877):775–778.

10 Cai K, Yin H, Qin QH, Li Y. Self-excited oscillation of rotating double-walled carbon nanotubes. *Nano Lett.*, 2014, **14**(5):2558–2562

11 Cai K, Li Y, Qin QH, Yin H. Gradientless temperature-driven rotating motor from a double walled carbon nanotube. *Nanotechnology*, 2014, **25**(50):505701.

12 Cai K, Yin H, Wei N, Chen Z, Shi J. A stable high-speed rotational transmission system based on nanotubes. *Appl. Phys. Lett.*, 2015, **106**(2):021909.

13 Novoselov KS, Geim AK, Morozov SV, Jiang D, Zhang Y, Dubonos SV, Grigorieva IV, Firsov AA. Electric field effect in atomically thin carbon films. *Science*, 2004, **306**(5696):666.

14 The Nobel Prize in Physics 2010, https://www.nobelprize.org/nobel_prizes/physics/laureates/2010/, (Retrieved Dec. 21, 2017)

15 Morozov SV, Novoselov KS, Katsnelson M I, Schedin F, Elias DC, Jaszczak JA, Geim AK. Giant intrinsic carrier mobilities in graphene and its bilayer. *Phys. Rev. Lett.*, 2008, **100**(1):016602.

16 Carlsson JM. Graphene: Buckle or break. *Nat. Mater.*, 2007, **6**(11):801–802.

17 Nair RR, Blake P, Grigorenko AN, Novoselov KS, Booth TJ, Stauber T, Peres NM, Geim AK. Fine structure constant defines visual transparency of graphene. *Science*, 2008, **320**(5881):1308–1308.

18 Xu XF, Pereira LFC, Wang Y, Wu J, Zhang KW, Zhao XM, Bae SK, Bui CT, Xie RG, Thong JDL, Hong BH, Loh KP, Donadio D, Li BW, Ozyilmaz B. Length-dependent thermal conductivity in suspended single-layer graphene. *Nat. Comm.*, 2014, **5**:3689.

19 Lee C, Wei X, Kysar JW, Hone J. Measurement of the elastic properties and intrinsic strength of monolayer graphene. *Science*, 2008, **321**(5887):385–8.

20 Zhong MY, Xu DK, Yu XG, Huang K, Liu XM, Qu YM, Xu Y, Yang DR. Interface coupling in graphene/fluorographene heterostructure for high-performance graphene/silicon solar cells.

Nano Energy, 2016, **28**:12–18.

21 Rebecca BC. Graphene maker aims to build British, billion-pound venture. *Daily Telegraph*, (1 July 2014)

22 Xu LQ, Wei N, Zheng YP, Fan ZY, Wang HQ, Zheng JC. Graphene-nanotube 3D networks: intriguing thermal and mechanical properties. *J. Mater. Chem.*, 2012, **22**(4): 1435−1444.

23 Varshney V, Unnikrishnan V, Lee J, Roy AK. Developing nanotube junctions with arbitrary specifications. *Nanoscale* 2018, **10**(1): 403-415.

24 Yang W, Yang W, Song AL, Sun G, and Shao GJ. 3D interconnected porous carbon nanosheet/carbon nanotube as polysulfides reservoir for high performance lithium-sulfur batteries. *Nanoscale* 2018, **10**(2): 816-824.

25 Jiang J-W, Leng J, Li J, Guo Z. Chang T, Guo X, Zhang T. Twin graphene: A novel two-dimensional semiconducting carbon allotrope. *Carbon*, 2017, **118**: 370-375.

26 Martins LGP, Matos MJS, Paschoal AR, Freire PTC, Andrade NF, Aguiar AL, Kong J, Neves BRA, de Oliveira AB, Mazzoni MSC, Filho AGS, Cançado LG. Raman evidence for pressure-induced formation of diamondene. *Nat. Comm.*, 2017, **8**:96.

27 Gao Y, Cao TF, Cellini F, Berger C, de Heer WA, Tosatti E, Riedo E, Bongiorno A. Ultrahard carbon film from epitaxial two-layer graphene. *Nat. Nanotechnol.*, 2018, **13**: 133-138.

28 Foroughi J, Spinks GM, Wallace GG, Oh J, Kozlov ME, Fang SL, Mirfakhrai T, Madden JDW, Shin MK, Kim SJ, Baughman RH. Torsional Carbon Nanotube Artificial Muscles. *Science* 2011, **334**: 494-497.

29 Lima MD, Li N, de Andrade MJ, Fang SL, Oh J, Spinks GM, Kozlov ME, Haines CS, Suh D, Foroughi J, Kim SJ, Chen YS, Ware T, Shin MK, Machado LD, Fonseca AF, Madden JDW,

Voit WE, Galvão DS, Baughman RH. Electrically, chemically, and photonically powered torsional and tensile actuation of hybrid carbon nanotube yarn muscles. *Science* 2012, **338**: 928-932.

30 Kim SH, Haines CS, Li N, Kim KJ, Mun TJ, Choi CS, Di JT, Oh YJ, Oviedo JP, Bykova J, Fang SL, Jiang N, Liu ZF, Wang R, Kumar P, Qiao R, Priya S, Cho K, Kim M, Lucas MS, Drummy LF, Maruyama B, Lee DY, Lepró X, Gao E, Albarq D, Ovalle-Robles R, Kim SJ, Baughman RH. Harvesting electrical energy from carbon nanotube yarn twist. *Science* 2017, **357**: 773-778.

31 Ebbesen TW, Hiura H. Graphene in 3-dimensions: Towards graphite origami. *Adv. Mater.*, 1995, **7**(6):582−6.

32 Feng J, Li WB, Qian XF, Qi JS, Qi L, Li J. Patterning of graphene. *Nanoscale*, 2012, **4**(16):4883.

33 Cai K, Cai HF, Yin H, Qin QH. Dynamic behavior of curved double-wall carbon nanotubes with rotating inner tube. *RSC Advances*, 2015, **5**(38): 29908-13.

34 LAMMPS, Molecular Dynamics Simulator. http://lammps.sandia.gov/ (Retrieved Dec. 21, 2017)

35 Stuart SJ, Tutein AB, Harrison JA. A reactive potential for hydrocarbons with intermolecular interactions. *J. Chem. Phys*. 2000, 112(14):6472−6486.

36 Jones JE. On the determination of molecular fields: II. From the equation of state of a gas. *Proc. Royal Society of London*, 1924, 106:463–77.

37 Thompson AP, Plimpton SJ, Mattson W. General formulation of pressure and stress tensor for arbitrary many-body interaction potentials under periodic boundary conditions. *J. Chem. Phys*. 2009, **131**(15):154107−6.

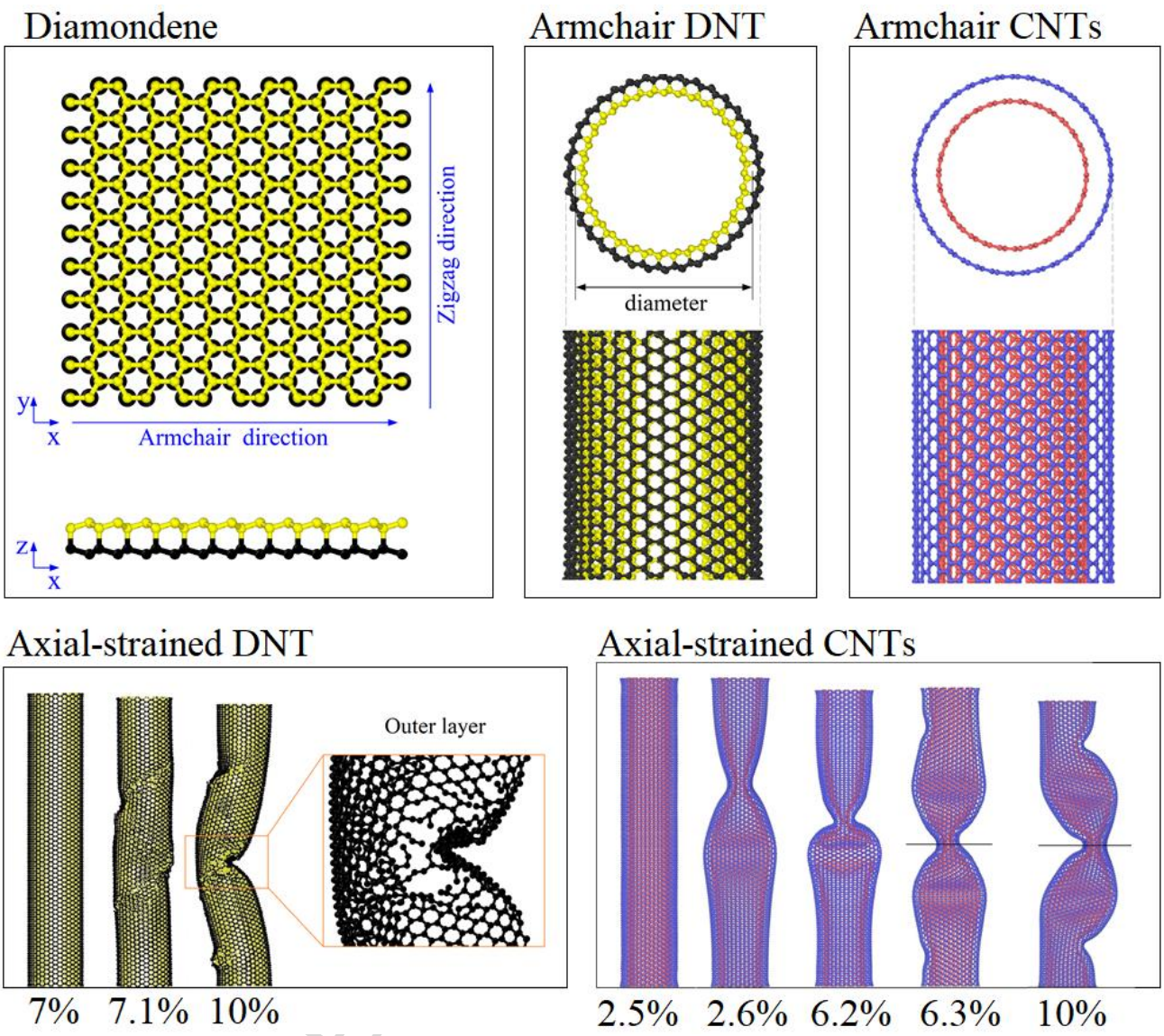

Graphical abstract

Highlights

1. The concept of a nanotube from diamondene is proposed.
2. The minimum radius for a stable armchair or zigzag DNT is predicted.
3. Under uni-axial compression, DNT has a critical buckling strain far greater than the double-walled CNTs with same average diameter.
4. Buckling happens due to the breakage of C-C bonds in the outer layer of DNT.
5. In buckling, a damaged DNT has only one mode, but the undamaged CNTs have more modes.